Journal of Power Sources 267 (2014) 48–57

Contents lists available at ScienceDirect

Journal of Power Sources

journal homepage: www.elsevier.com/locate/jpowsour

Study on effect of poly (ethylene oxide) addition and in-situ porosity generation on poly (vinylidene fluoride)-glass ceramic composite membranes for lithium polymer batteries

Nageswaran Shubha [a], Raghavan Prasanth [a, b], Huey Hoon Hng [a], Madhavi Srinivasan [a, b, *]

[a] School of Materials Science and Engineering, Nanyang Technological University, Block N4.1, 50 Nanyang Avenue, Singapore 639798, Singapore
[b] Energy Research Institute @ NTU (ERI@N) Research Techno Plaza, 50 Nanyang Drive, 637553, Singapore

HIGHLIGHTS

- Effect of in-situ porosity generation on PEO/PVdF-LAGP polymer electrolytes is studied.
- Preferential dissolution process generates in-situ porosity on electrospun fibers.
- In-situ porosity generation improved conductivity and electrochemical properties.
- Incorporation of LAGP improved the mechanical properties of PEs.
- Li/$LiFePO_4$–C cell with composite electrolyte showed stable cycling performance.

ARTICLE INFO

Article history:
Received 28 March 2014
Received in revised form
12 May 2014
Accepted 13 May 2014
Available online 22 May 2014

Keywords:
Polymer electrolyte
Lithium ion batteries
Polymer blend
In-situ porosity generation
Electrospinning

ABSTRACT

The effect of blending polyethylene oxide with poly (vinylidene fluoride)–lithium aluminum germanium phosphate (LAGP) composite and in-situ porosity generation on the electrochemical performance of polymer electrolytes based on non-woven fibrous mats is studied. Electrospinning process parameters are controlled to get a fibrous membrane consisting of bead-free, multilayered, three dimensional network structure of ultrafine fibers. The electrospun membranes are subjected to a preferential polymer dissolution process to prepare a highly porous structure. The membranes show high surface roughness with uniformly sized and distributed pores on the fibers. The membranes with good mechanical strength, thermal stability and high porosity exhibit high swelling when activated with liquid electrolyte. The prepared composite polymer electrolytes show high ionic conductivity. The addition of the glass ceramic improves the mechanical and thermal stability, while blending and in-situ porosity generation improves the ionic conductivity, charge–discharge performance, cycling stability, interface properties and compatibility with lithium electrode.

1. Introduction

Solid polymer electrolytes have received widespread attention due to their excellent processability, flexibility, safety and dimensional stability. Although solid polymer electrolytes have many advantages, they suffer from low ionic conductivity at room temperature which limits their practical application. Currently commercially used liquid electrolytes offer high ionic conductivity, but leakage and flammability are the main concern. Gel polymer electrolytes which combine the advantages of both (liquid and solid polymer electrolytes) are closer to practical application, when compared to solid polymer electrolytes [1]. Gel polymer electrolytes (GPEs) possess both the cohesive properties of solids and diffusive property of liquids [2]. GPEs are prepared by immersing a polymeric film into a mixture of a lithium salt in a low molecular weight solvent system. Upon gelling these electrolytes predominantly show three phases: solid polymer matrix, gelled polymer phase and absorbed liquid electrolyte encapsulated in the pores and cavities of the host membrane [3]. Conductivity of the GPE is mainly influenced by the gelled phase and liquid phase, while the solid phase contributes towards improving mechanical strength. The mechanism of ion transport in GPEs is diffusion through the

* Corresponding author. School of Materials Science and Engineering, Nanyang Technological University, Block N4.1, 50 Nanyang Avenue, Singapore 639798, Singapore. Tel.: +65 67904606; fax: +65 67909081.
E-mail address: madhavi@ntu.edu.sg (M. Srinivasan).

http://dx.doi.org/10.1016/j.jpowsour.2014.05.074
0378-7753/

solvent system, while in solid polymer electrolytes, the ion motion is due to local movement of the polymeric chain above its glass transition temperature [4]. Although the ionic conductivity of GPEs is predominantly influenced by diffusion, complexation of lithium salts with the polymer leads to the involvement of local relaxation of the polymer as well [4]. Previous studies have shown that by blending polymers, a proper balance between improving ion dissociation and localized polymeric motion can be achieved [5]. For achieving best electrochemical performance in GPEs an increase in the gelled polymer phase and absorbed liquid electrolyte encapsulated in the pores and cavities of the host polymer matrix is necessary [4,6,7]. Increasing porosity is one of the reported ways to increase the content of the gel phase. A highly porous membrane exhibits high ionic conductivity, but at the same time, increase in porosity may lead to a decrease in mechanical strength. Composite polymer electrolytes, which incorporate ceramic fillers to help improve the dimensional stability, have gained prominence recently to tackle the loss of mechanical strength associated with highly porous GPEs. The addition of ceramic fillers has also been reported to significantly enhance the performance of GPEs [8–14].

Several polymers have been studied as host polymers for preparing polymer electrolytes. Amongst them, poly(ethylene oxide) (PEO) and polyvinylidene fluoride (PVdF) have been widely studied as matrices for solid and gel polymer electrolytes respectively [15,16]. The presence of ether linkages in PEO leads to local relaxation and segmental motion of the polymeric chains which facilitate lithium ion conduction, when it is used as polymer electrolytes in lithium ion batteries [15]. The unique properties of PVdF such as good electrochemical stability, high dielectric constant (~8.4) and presence of strong electron withdrawing fluorine make it a good candidate for the preparation of electrolyte cum separator for lithium ion batteries [16].

The effect of blending PEO with PVdF to improve the segmental motion, dissociation of lithium salts and improve the electrochemical performance of the resulting GPE has been reported previously [5]. In the GPE, the presence of PVdF retains the mechanical properties of the membrane, while the ether linkages in PEO help to improve the segmental motion and dissociation of lithium salts. Electrospinning was used to prepare the non-woven fibrous mats by the interlaying of ultrafine fibers providing fully interconnected pathways for ion transportation. Electrospun membranes show high porosity (>80%) and high electrolyte uptake [5]. In the current study, a preferential polymer dissolution process is adopted to remove PEO from the composite polymer membrane to generate in-situ porosity on the electrospun PEO/PVdF-glass ceramic composite fibers. The in-situ porosity generation helps to increase the electrolyte absorption capability and swelling ability of the membrane, while lithium aluminum germanium phosphate (LAGP) (glass ceramic) increases the thermal stability, mechanical stability and lithium ion concentration. The incorporation of LAGP into the polymer improves the physical properties and maintains the integrity of the composite polymer electrolyte after swelling [17]. The effect of in-situ porosity generation on the ionic conductivity and electrochemical properties of glass ceramic composite electrolyte is studied.

2. Experimental

2.1. Materials for preparation of LAGP

$CH_3CO_2Li\cdot 2H_2O$ (99%, Alfa Aesar), $AlN_3O_9\cdot 9H_2O$ (98%, GCE Chemicals), P_2O_5 (95%, Fisher Scientific), $C_2H_4O_2$ (99.5%, Fisher Scientific), $Ge(CH_3O)_4$ (95%, Sigma Aldrich), $C_6H_8O_7$ (99.5%, GCE Chemicals) and $C_2H_6O_2$ (99.5%, Merck) were used as received.

2.2. Sol gel synthesis of LAGP

The NASICON type LAGP was prepared by sol–gel method as reported previously [18,19]. In a typical experiment, $CH_3CO_2Li\cdot 2H_2O$, $AlN_3O_9\cdot 9H_2O$ and P_2O_5 were weighed in stoichiometric proportions and dissolved in ethylene glycol (0.001 mol of LAGP:100 ml of ethylene glycol) and heated at 90 °C with continuous stirring. Acetic acid ($C_2H_4O_2$) (0.001 mol of LAGP:10 ml of acetic acid) was then added into the mixture. The mixture was stirred until a clear solution was obtained, then required amount of $Ge(CH_3O)_4$ was added and the solution was stirred for 5 min. Following that, powder citric acid (CA) $C_6H_8O_7$; gelation agent (4 mol of CA:1 mol of LAGP) was added to promote polyesterification and polycondensation and stirred continuously for 1 h to obtain a clear final solution. The final solution was heated at 100 °C until gelation was complete. The gel was then placed in an alumina crucible and heated to 900 °C at a ramping rate of 2 °C min^{-1} with a 10 h dwelling time under ambient conditions. The resulting powder was then collected and used as the glass ceramic filler after ball milling to reduce the particle size.

2.3. Preparation of PEO/PVdF-LAGP composite membrane

PVdF (M*w*; 53,4000, Sigma Aldrich) and PEO (M*v*; 100,000 Sigma Aldrich), were vacuum dried at 60 °C for 6 h before use. Solvents, acetone and *N*,*N*-dimethyl acetamide (DMAc) (HPLC grade, Aldrich) were used as received. Prior to the composite preparation, LAGP was uniformly dispersed in DMAc using mortar and pestle for proper distribution of glass ceramic particles in the composite. For preparation of the composite, right proportion of PVdF and LAGP dispersion were added in a mixed solvent of Acetone/DMAc (7:3 w/w) (weight ratio between PVdF and LAGP is kept constant at 94:6). To the resulting composite solution (PVdF–LAGP), required amount of PEO (5, 10 and 20 wt.%) was added and the solution was stirred for 24 h at room temperature to get the final composite solution. The solid content for the final solutions were carefully kept at 16 wt.%. The LAGP content in the composite was kept constant at 6 wt.% with respect to PVdF, to keep the ratio of PVdF to LAGP constant in the membrane after preferential leaching out of PEO. For example; 100 g of ESM-01 solution contains 89.3 g of PVdF, 5.7 g of LAGP and 5 g of PEO. The solution was left in an air tight container for 15 min to get bubble free clear solution for electrospinning. The solution was fed to the syringe fitted with a blunt stainless steel needle having bore size of 0.6 mm, connected to a high voltage source using a syringe infusion/withdrawal pump (KD Scientific, Model-210). The distance between the tip of the needle and the collection drum was kept at ~20 cm. The solution feed rate (0.2 ml min^{-1}) and the collector drum rotation speed (150 rpm) was kept constant. Depending on the amount of PEO in the spinning solution, the applied voltage was varied from 18 to 20 KV to get uniform fibers with bead free morphology. The fibers were collected as a free standing non-woven membrane on a thin aluminum foil wrapped over the grounded rotating drum. The average thickness of the membrane was carefully controlled to ~150 μm. Before removing the membrane from the collection drum, it was dried at room temperature for 12 h to prevent the shrinking of fibers. The as spun membranes were designated as ESM-01, ESM-02 and ESM-03 for electrospun membrane based on PEO blended with PVdF-LAGP composite with PEO content (wt.%) 5, 10 and 20 to highlight their respective composition.

2.4. Preparation of in-situ porosity generated membrane

The electrospun membranes (ESM-01, ESM-02 and ESM-03) were immersed in a heated water bath (70 °C) for 48 h to leach

out PEO from the micron sized fibers. PEO is water soluble, while PVdF is not; therefore PEO was preferentially isolated and removed from the membranes. The membranes were then dried in an air oven at 60 °C followed by vacuum drying at 80 °C for 24 h. The dried membranes were transferred to a dry box at 25 °C (H_2O level < 20 ppm) for further characterization and use. The in-situ porosity generated membranes obtained from ESM-01, ESM-02 and ESM-03 were designated as IPG-01, IPG-02 and IPG-03 respectively.

2.5. Characterization of PEO/PVdF-LAGP composite membranes

The membranes were characterized for surface morphology, average fiber diameter, porosity, thermal properties and mechanical properties. Surface morphology of the membranes was examined with high resolution field-emission scanning electron microscope (FE-SEM: JEOL JSM7600F) at an accelerating voltage of 15 kV. Nearly 300 fibers were examined for estimating the average fiber diameter (AFD). Porosity (P) of the membrane was determined following the procedure reported previously, using the equation

$$P(\%) = \frac{M_{BuOH}/\rho_{BuOH}}{M_{BuOH}/\rho_{BuOH} + M_m/\rho_P} \times 100$$

where M_m, M_{BuOH}, ρ_{BuOH} and ρ_P are the mass of the dry membrane, mass of n-butanol absorbed, density of n-butanol and density of polymer, respectively [13].

Thermal properties were evaluated by differential scanning calorimetry (DSC: Q10, TA Instruments) and thermo gravimetric analysis (TGA: Q500 TA Instruments) at a heating rate of 10 °C min^{-1} under N_2 atmosphere from room temperature to 350 °C and 700 °C respectively. The crystallinity of the samples were calculated from the DSC data as reported elsewhere [5,20]. Mechanical properties of the membranes with average thickness of 150 μm were measured by universal testing machines (UTM, Instron 5567 Instruments). Tensile strength, Young's modulus and percentage elongation were evaluated using die punched dumbbell shaped samples as per ASTM D 638 using type V die. The extension rate was kept at 5 mm min^{-1}. The dimensions of the sample used were 15 × 2 cm.

2.6. Electrochemical characterization

The composite membranes were transformed into composite polymer electrolyte (CPE) by activating a circular piece (area ~2 cm^2) with 1 M LiTFSI in EC:DEC (1:1 w/w). The membranes were immersed in the electrolyte solution and electrolyte uptake (δ) (ability to absorb electrolyte) was calculated as reported [5]. The leakage properties of the soaked CPEs were measured according to the procedure reported by Kim et al. [21]. The fibrous membranes were immersed in the electrolyte solution for 2 h to ensure it reached a state of equilibrium. After removal of the excess liquid electrolyte that remained on the surface, the membranes were placed between two filter papers and squeezed by pressing with a standard weight (pressure of 720 N m^{-2}). The weight changes of the membranes were measured under equal time interval (15 min) and the leakage of the electrolyte was calculated using the equation:

$$R = \mathrm{MPE}/\mathrm{MPE}_{,\mathrm{saturated}}$$

where R is the relative absorption ratio of the liquid electrolyte, $\mathrm{MPE}_{,\mathrm{saturated}}$ is the mass of the CPE when the membrane is fully saturated with the liquid electrolyte, and MPE is the mass of the CPE after a time interval when the saturated composite polymer electrolyte is squeezed by pressing between the filter papers.

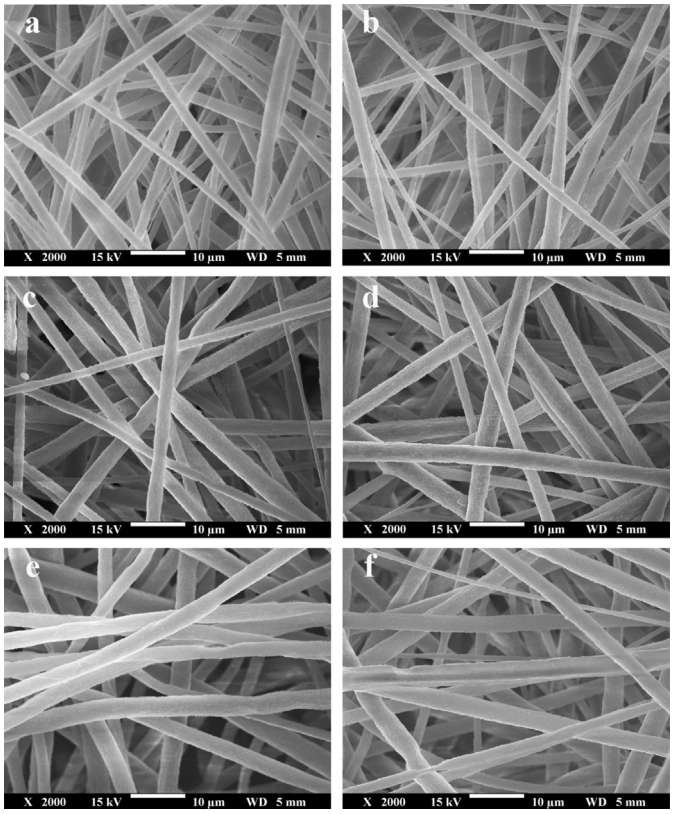

Fig. 1. Surface morphology of electrospun membranes; (a) ESM-01, (c) ESM-02, (e) ESM-03, (b) IPG-01, (d) IPG-02 and (f) IPG-03.

Ionic conductivity of the CPEs was measured between −20 and 70 °C by AC impedance method. The time dependant interfacial resistance (R_f) between lithium electrode and CPE was evaluated by monitoring the complex impedance response, on Li/CPE/Li symmetrical cells over a period of 12 days. The ionic conductivity and R_f measurements were performed in a Swagelok® cell at an amplitude of 20 mV over the frequency range 10 mHz–1 MHz using Solartron 1470E and SI 1255B Impedance/gain-phase analyzer coupled with a potentiostat. The SS/CPE/SS cells were placed in a temperature controlled environmental chamber and kept at each temperature for 30 min prior to ionic conductivity measurement to ensure thermal equilibrium. Ionic conductivity (σ) was calculated as $\sigma = t/R_bA$; where t and A denote the thickness and net available area (product of porosity and area of the CPE), respectively and R_b is the bulk resistance obtained from the x-axis intercept of the complex AC impedance response with frequency [5].

Two-electrode electrochemical coin cells were fabricated by placing the CPE between lithium metal anode (~300 μm thick) and carbon-coated lithium iron phosphate ($LiFePO_4$) cathode (~23 μm thick). The composite cathode was formulated by mixing active material, conducting additive (Super P Li carbon by Timcal) and PVdF binder (Sigma Aldrich) in the ratio 80:10:10 using N-methyl pyrrolidinone (NMP) as solvent for binder to form slurry. The resulting viscous slurry was subsequently coated over aluminum foil using doctor blade technique. The resulting electrode was then dried in a vacuum oven at 80 °C for several hours to completely remove the solvent and then pressed in between twin rollers to provide necessary adherence of the coating to the current collector. The dried electrodes were then punched into circular discs of 16 mm diameter. Before cell assembly, the composite cathode was

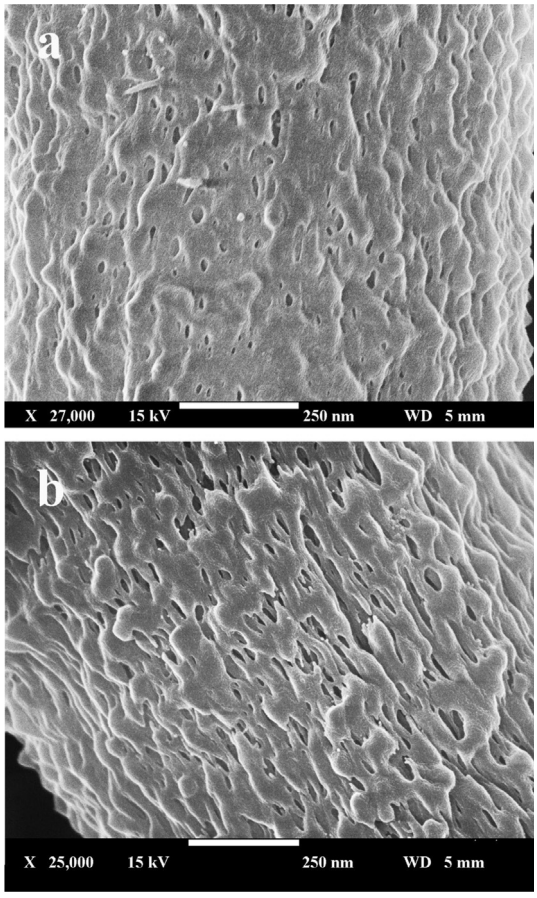

Fig. 2. Magnified images of surface morphology of electrospun fibers; (a) IPG-02 and (b) IPG-03.

dried in a vacuum oven at 80 C for 12 h to remove residual solvent traces (if any). The test cells, Li/CPE/$LiFePO_4$ were fabricated in CR2016 coin cell and the galvanostatic charge–discharge tests were conducted using battery testing system (BTS XWJ, Neware Tech. Co.), between 2.5 and 4.0 V at room temperature at various C rates. The activation of electrospun membrane to prepare CPE and the fabrication of test cells were carried out in an argon-filled glove box with oxygen and moisture level <0.1 ppm.

3. Results and discussion

3.1. Membrane morphology, porosity, electrolyte uptake and retention

Fig. 1(a–f) shows the surface morphology of the electrospun membranes before and after in-situ porosity generation. The membranes consist of multilayered, three dimensional network of fine fibers with uniform non-beaded morphology and high surface roughness. The interlaying of fibers provides good mechanical strength to the fibrous membrane. The observed surface roughness is beneficial for better adhesion with the electrode and improved interfacial properties [5]. It is seen that the amount of PEO blended into the composite has an effect on the average fiber diameter of the membranes. With increasing PEO content in the composite, the fiber diameter increases slightly. The AFD of the ESM membranes is 1.9, 2.3 and 2.7 μm for ESM-01, ESM-02 and ESM-03 respectively. This can be attributed to the higher voltage used to electrospin the membranes and the increased viscosity due to the addition of PEO [5]. The higher applied voltage ejects more fluid in the jet which leads to deposition of fibers with larger diameter [13]. The AFD of the membranes after in-situ pore generation is found to be slightly lower than the as spun membranes (ESMs). This effect is more pronounced with increasing PEO content. The AFD of the membranes after in-situ porosity generation is 1.8, 2.1 and 2.4 μm for IPG-01, IPG-02 and IPG-03 respectively.

Fig. 2(a) and (b) shows the magnified image of IPG-02 and IPG-03. The images show that pores are uniformly distributed on the surface of the fibers, with IPG-03 having a more porous surface, attributed to the higher PEO content in the blend. The uniformly distributed pores on the fiber surface indicate that the blending PVdF and PEO results in a uniform solution. The presence of large number of pores on the surface of the fiber confirms that PEO has been successfully leached out from the membrane by the preferential dissolution process. It is observed that the surface roughness of the membranes is enhanced by in-situ porosity generation. This increased surface roughness and porosity is beneficial for higher electrolyte uptake and enhanced electrochemical properties.

Porosity is one of the key factors which determine the performance of polymer electrolytes based on electrospun membranes in lithium ion batteries [22]. Higher porosity can enlarge the contact area between the polymer and liquid electrolyte, which ensures that the electrolyte is well retained in the polymer membrane. Porosity of the prepared membranes is determined by *n*-butanol uptake method. The *n*-butanol does not interact with the membrane; rather it penetrates the pores and occupies all the available pores, and thus gives a measure of the total pore volume of the membrane. The porosity of the composite membranes before and after in-situ porosity generation is tabulated in Table 1. IPG-03 membrane exhibits the highest porosity while ESM-01 shows the lowest porosity. It is observed that the porosities of all the membranes are 85 ± 5%. The narrow range of porosity of the membranes is attributed to the close similarities in the membrane morphologies and interlaying of fibers. Porosity also depends on the AFD, which strongly depends on the solution concentration and applied voltage. Lower viscosity solution forms fibers with lower AFD which results in loose packing of the fibers, leading to higher porosity [13]. However, in this study, the membrane with lower AFD showed slightly lower porosity. After in-situ porosity generation the membranes showed higher porosity compared to the as spun composite membranes, which also depends on the amount of PEO present in the original blend. Therefore IPG-03 (highest PEO content, 20 wt.%) has higher porosity compared to IPG-01 and IPG-02.

The electrolyte uptake and retention of the IPG membranes in 1 M LiTFSI in EC:DEC (1:1 w/w) is studied for a period of 1 h. The electrolyte uptake is strongly dependent on porosity, pore size, pore volume and pore density. It is seen that the electrolyte uptake for IPG-01, IPG-02 and IPG-03 follows the same trend as the porosity

Table 1
Properties of ESM and IPG membranes activated with 1 M LiTFSI in EC:DEC (1:1 w/w).

Membrane	Porosity (%)	Electrolyte uptake (%)	Crystallinity (%)	Ionic conductivity at 30 °C (mS cm^{-1})
ESM-01	78	632	39.1	6.3
ESM-02	80	652	40.4	7.0
ESM-03	83	703	42.6	7.7
IPG-01	85	723	36.8	8.0
IPG-02	89	768	38.2	9.1
IPG-03	93	831	38.8	10.9
PVdF-PEO[a] (90:10)	80	750	42.3	4.9

[a] Adapted from Ref. [5].

with IPG-03 having the highest electrolyte uptake (Fig. 3(a)). The high uptake is due to the high porosity and surface roughness of the IPG membranes. It is observed that the uptake process is rapid and is almost stabilized within 15 min which can be attributed to the high porosity, fully interconnected open pore structure, interlaid fiber structure of the membranes and good affinity to the electrolyte. The electrospun membrane displays sufficient mechanical strength and easy handleability even after activation with electrolyte.

The highly porous structure and the high electrolyte uptake will naturally lead to a speculation about the ability of the membranes to retain the absorbed electrolyte over time. Fig. 3(b) shows the electrolyte retention of the IPG membranes. It is seen that all the membranes show high electrolyte retention with a leakage <15%, after 2 h. The high electrolyte retention by the composite polymer electrolytes may be due to the combined effect of good affinity of the membrane to electrolyte, high surface roughness, large surface area and tailored pore structure of the membranes.

3.2. Thermal and mechanical characterization

The effect of adding low melting point PEO to PVdF–LAGP composite on the thermal stability of the electrospun membranes is studied using TGA and DSC. Fig. 4(a) shows the DSC plots of ESM and IPG membranes. Pristine PEO and PVdF show a melting endotherm at 65 °C and 158 °C respectively [5]. It is seen that ESM-02 and ESM-03 exhibits the characteristic peaks of both PEO and PVdF at 61 and 156 °C respectively, while only one characteristic endotherm peak is observed for ESM-01 at ~156 °C. This implies the microphase separation is accomplished in the syringe when the composite solution containing higher PEO content (≥10 wt.%) is kept without stirring for long time while spinning [23]. The slight lowering of crystalline melting temperature (T_m) of ESM is due to the presence of LAGP particles that inhibit effective reorganization of polymer chains [17,24]. Only one melting endotherm is observed for all IPG membranes with T_m of ~156 °C, which indicates leaching out of PEO from the membrane by in-situ pore generation. The melting temperature of pristine PVdF is 158 °C, while the electrospun composite membranes with LAGP have slightly lower melting points (~156 °C). The addition of ceramic fillers ($BaTiO_3$ and Al_2O_3) barely influences the melting temperature of the polymer matrix, as reported earlier [25]. However the small change in the melting points of the composite membranes probably results from lower crystallinity due to the association between the ceramic particles and polymer.

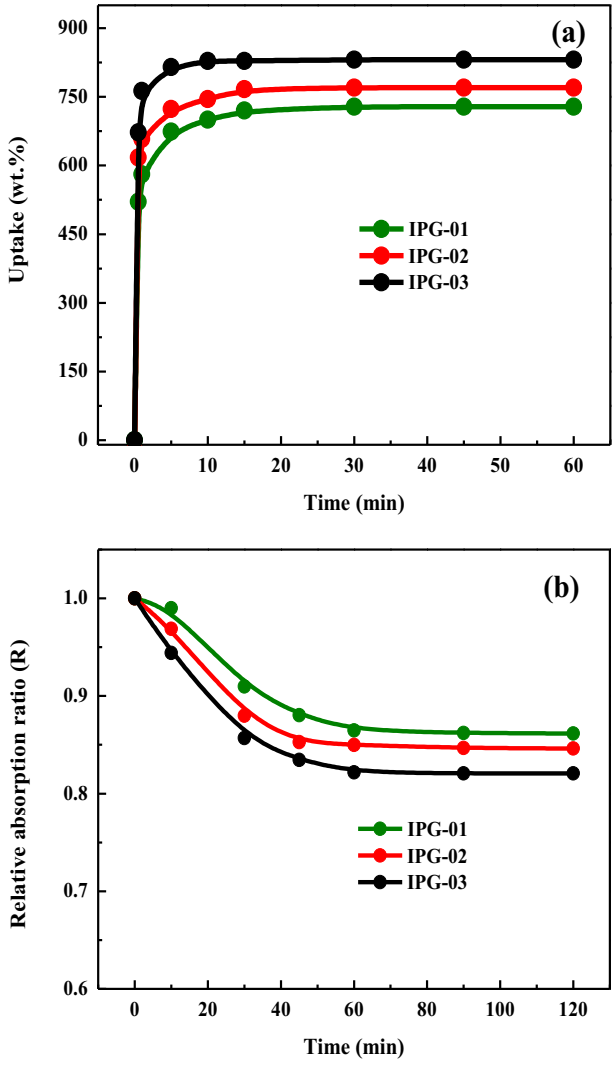

Fig. 3. (a) Electrolyte uptake (%) and (b) Relative absorption ratio of IPG membranes (1 M LiTFSI in EC:DEC, 1:1 w/w).

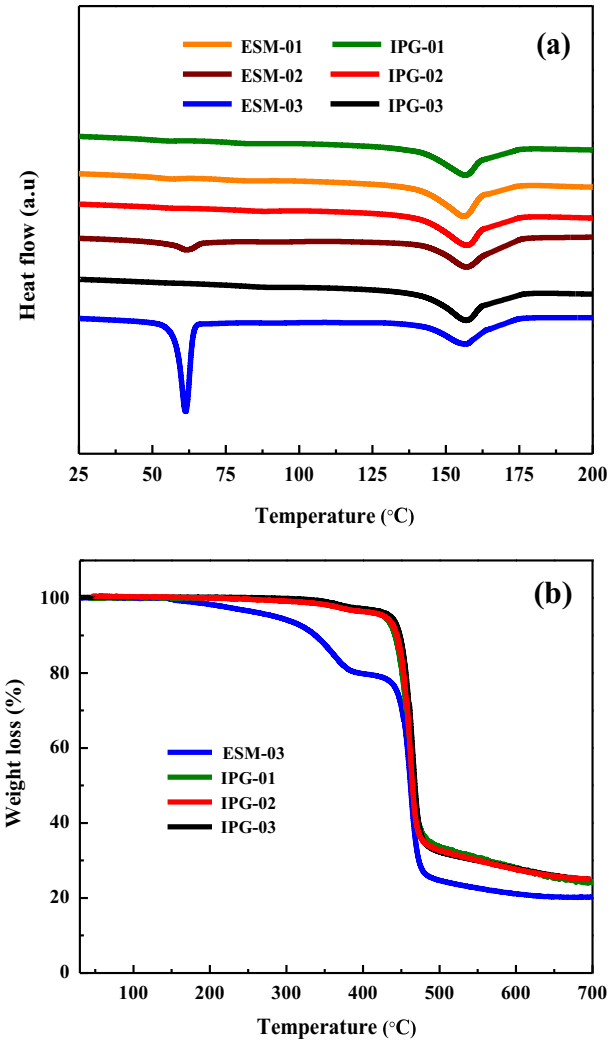

Fig. 4. (a) DSC traces, and (b) TGA traces of electrospun membranes under N_2 atmosphere at a heating rate of 10 °C min^{-1}.

The endotherm corresponding to PEO in the composite membrane (ESM) is very shallow when compared to pristine PEO proving that crystallinity of PEO has been reduced by the incorporation of LAGP into the composite membrane. For the IPG membranes, the peak corresponding to PEO is no longer seen, proving that PEO has been completely leached out from the as spun membranes. The crystallinity of the ESM and the IPG membranes are tabulated in Table 1. It is seen that the crystallinity of the composite membranes increase with increasing PEO content. The composite membrane shows lower crystallinity than PVdF/PEO blend membrane without LAGP [5]. The observed difference in the crystallinity arises from the inhibition of crystallization by the LAGP glass ceramic during the solidification process of the fiber, which reduces the volume fraction of the crystalline phase in the fiber [17]. The surface charges on the ceramic particles also contribute to increasing the amorphous phase of the polymer as a result of higher nucleation rate during the solidification process by acting as facile nucleation centers [26]. The increase of amorphous regions in the polymer is beneficial for achieving a higher ionic conductivity [11–13]. It is reported that the crystallinity of electrospun membranes are higher than pristine polymer due to the orientation of the polymer to the fiber axis when it drawn to form nanofibers [12,13]. However in the present study all the membranes (more evident in the case of IPG) showed lower crystallinity than pristine PVdF powder (40.5%) [5]. This observation confirms that the addition of LAGP inhibits the crystallization process of the polymer during spinning and subsequent solidification process. The crystallinity of IPG membranes is slightly lower than ESM membranes, which results from leaching out highly crystalline PEO from the composite membrane.

The TGA curves of the electrospun membranes are shown in Fig. 4(b). It is seen that the TGA curves of the ESM membrane shows characteristic two step weight loss, with the first short peak at a temperature ~324 °C and longer peak at 438 °C corresponding to the decomposition temperature of PEO and PVdF respectively. The decomposition temperature of pristine PEO and PVdF are found to be 318 and 419 °C respectively [5]. Shift of thermal decomposition temperature toward higher temperature range confirms enhancement in thermal stability of the composite [17,24]. The onset decomposition temperature of ESM is found to be ~170 °C and at a temperature of 386 °C, PEO is completely decomposed. At 700 °C, a char yield of 19% is observed for ESM-03 membrane, which is about 83% char yield of pristine PVdF, proving that prepared electrospun membrane has good thermal stability [5]. The char yield of PVdF at 700 °C is 25%. The IPG membranes show similar thermogram profiles as pristine electrospun PVdF [5]. It is observed that all IPG membranes show close onset decomposition temperature (~435 °C) which is significantly higher than ESM membrane. A slight decomposition peak at ~360 °C observed for IPG membranes may be due to the presence of negligible amount of PEO traces in the membrane after in-situ porosity generation process. A char yield of about 25% is observed for all IPG membranes at 700 °C

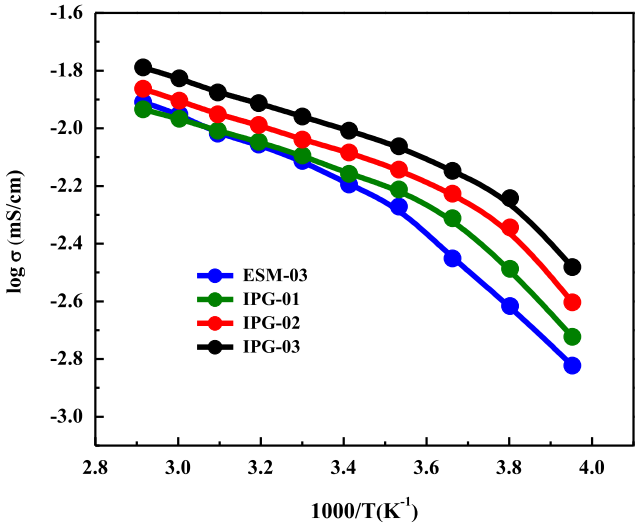

Fig. 5. Temperature dependant ionic conductivity of IPG membranes activated with 1 M LiTFSI in EC:DEC (1:1 w/w).

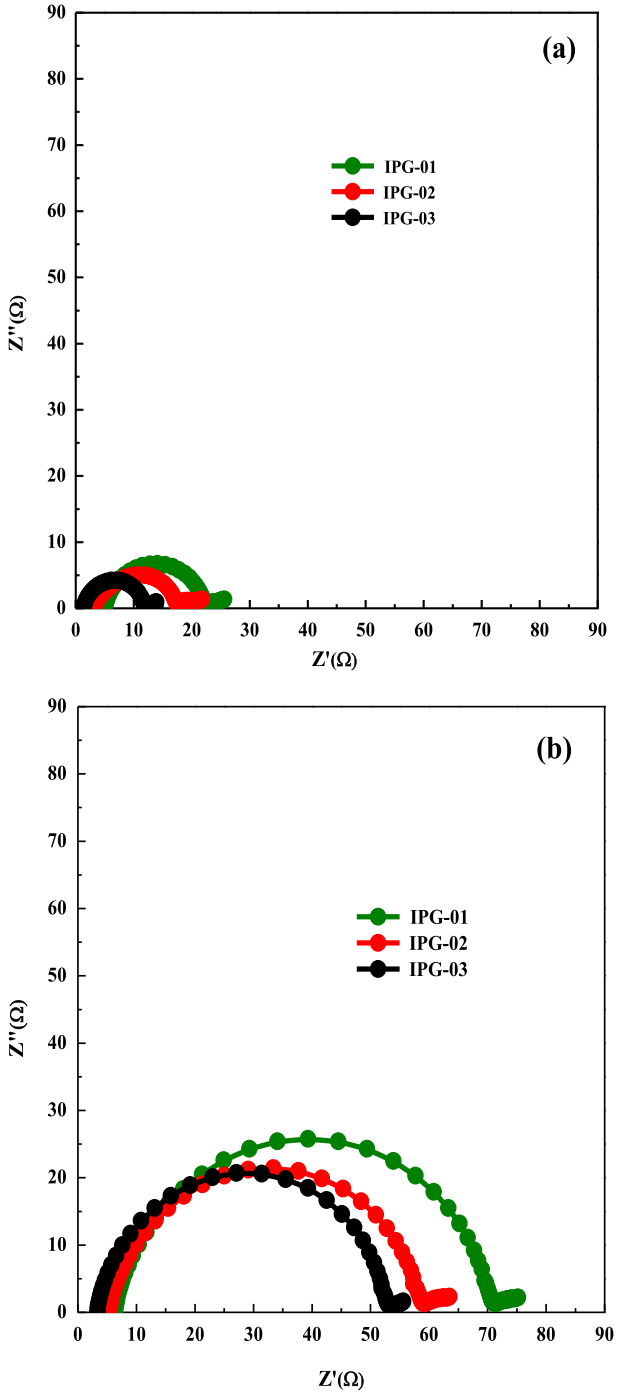

Fig. 6. AC impedance spectra of composite polymer electrolytes based on IPG membranes (Li/CPE/Li cells, 10 mHz–1 MHz): (a) initial impedance and (b) impedance after12days storage.

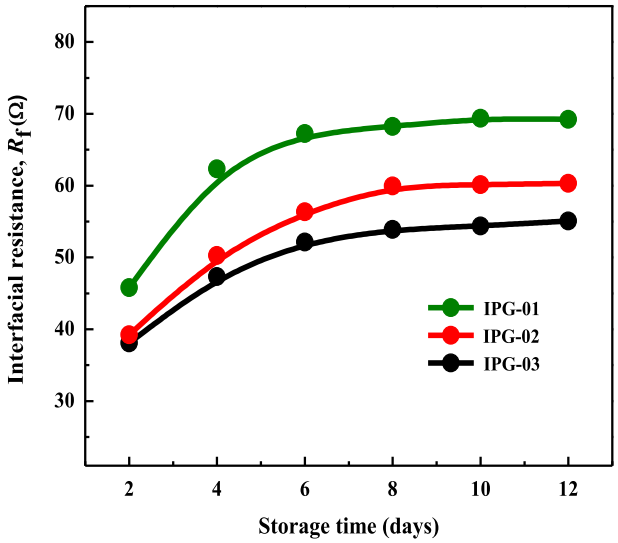

Fig. 7. Time dependant interfacial behaviors of composite polymer electrolytes based on IPG membranes (Li/CPE/Li cell, frequency range 10 mHz–1 MHz).

which is about 6% higher than the corresponding ESM membrane indicating that PEO is leached out during in-situ porosity generation.

The lowered crystallinity and increased porosity of the IPG membranes leads to doubts on the mechanical stability of the membranes. Mechanical strength of electrospun PVdF/PEO (80:20 w/w) blend membrane incorporated with 6 wt.% LAGP before and after leaching out PEO from the membrane is studied using ESM-03 and IPG-03 and compared with the PVdF/PEO blend membrane without LAGP. It was found that incorporation of LAGP enhances both ultimate tensile strength and Young's modulus of the membranes, which is attributed to reinforcing effect of inorganic component dispersed in the polymer matrix [13]. PVdF/PEO (80:20 w/w) blend membrane with 6% LAGP before (ESM-03) and after (IPG-03) leaching out the PEO from the membrane showed Young's modulus of 14.8 and 15.9 MPa respectively, while the Young's modulus of corresponding PVdF/PEO blend membrane without LAGP is found to be 9 MPa, which is about 40% lower than the membrane with LAGP. Similarly, the ultimate tensile strength of ESM-03 (9.3 MPa) and IPG-03 (10.1 MPa) is 60–75% higher than PVdF/PEO blend membrane without LAGP (5.8 MPa). Thus it is confirmed that incorporation of LAGP in the composite membrane contributes towards improving the mechanical properties.

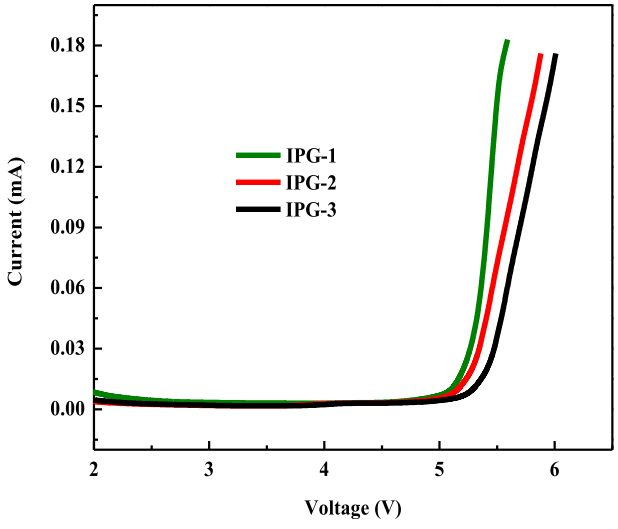

Fig. 8. Anodic stability by LSV of composite polymer electrolytes based on IPG membranes (Li/CPE/SS cells, 1 mV s^{-1}, 2–5.5 V).

3.3. Ionic conductivity

The temperature dependent ionic conductivity of the CPEs activated with 1 M LiTFSI in EC:DEC (1:1 w/w) between −20 and 70 °C is studied and shown in Fig. 5. AC impedance spectra of all the samples comprised of only a spike and the bulk resistance of the sample was obtained from the intersection point of the spike at the real axis of the Nyquist plot. A smooth increment in ionic conductivity is observed with increasing temperature. The ionic conductivity of the CPEs at 30 °C follows the order IPG-03 > IPG-02 > IPG-01 or ESM-03 > ESM-02 > ESM-01. It is seen that the ionic conductivity of IPG membranes is higher than the ESMs, suggesting that in-situ generated porosity has a more pronounced effect on ionic conductivity when compared to addition of PEO. It is seen that ionic conductivity follows the same trend as the porosity. Higher porosity leads to higher electrolyte uptake which results in higher ionic conductivity. The ionic conductivity of the CPE is dependent on number of charge carriers as per the equation $\sigma = \Sigma N_i R_i \dot{E}_i$, where N_i, R_i and $\dot{E}_i$ are number of charge carriers, ionic charge and ionic mobility, respectively. Higher swelling implies larger number of free charge carriers translating to higher ionic conductivity. Amongst all the samples, IPG-03 shows the highest ionic conductivity. This can be attributed to the higher porosity, electrolyte uptake, lower crystallinity, higher surface area, increased number of lithium ions due to the presence of LAGP and weakening of the polymer–cation association because of the glass ceramic particles [27]. The ionic conductivities of the ESM and IPG membranes at 30 °C are tabulated in Table 1. It was also observed that ionic conductivity of PVdF/PEO (90:10) blend membrane (4.9 mS cm^{-1} at 30 °C) is lower than the corresponding polymer electrolyte with LAGP [5]. The difference in ionic conductivity can be attributed to higher amorphous content of the polymer in the composite and the Lewis acid–base interactions between the filler and polymer chains [11–13,27]. The high conductivity of LAGP also contributes to the total conductivity of the composite electrolyte [28]. LAGP acts as a source of lithium ions thereby increasing the number of active charge carries, also the presence of Lewis acid–base interactions reduces the ion–ion coupling, leading to increased lithium ion dissociation [11,13]. The surface functional group (O/OH) of the glass ceramic can compete with the F atoms of PVdF to form Lewis acid–base complexes with Li ion, which leads to the weakening of the complexation between Li ions and F atoms of the PVdF chain thereby promoting Li ion diffusion [29,30]. The as prepared LAGP shows an ionic conductivity of 4.8×10^{-3} Scm^{-1}. This value is significantly higher than the earlier reports [31,32]. The difference in conductivity may be due to the difference in synthesis method and conditions adopted in the different studies.

All the CPEs studied here show smooth enhancement in conductivity with increasing temperature. This is due to the increasing number of charge carriers due to the higher lithium salt dissociation and increase in mobility of Li^+ ions due to lowering of the energy barrier with temperature. It is noticed that sharp increase in ionic conductivity occurs at lower temperatures. This can be assigned to the high self-dissociating and ion-transporting abilities of LiTFSI in EC:DEC electrolyte at low temperatures [33]. Additionally, the high porosity of the electrospun membranes and more significantly the interconnectivity of micron-sized pores, assist the easy migration of ions which results in high ionic conductivity even at low temperatures [34]. It is also observed that the ionic

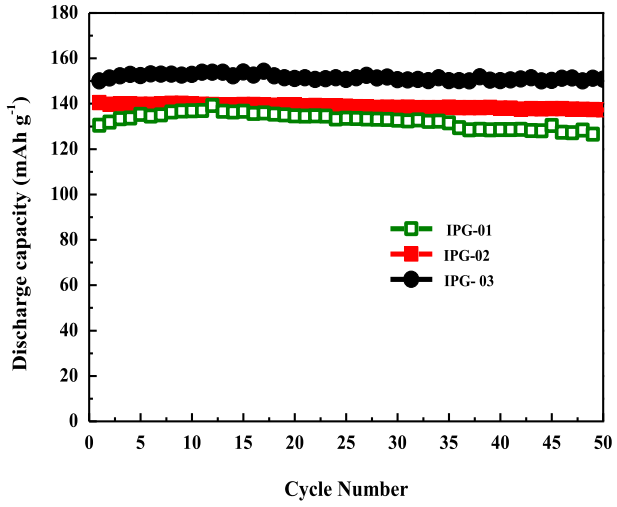

Fig. 9. Cycling properties of Li/$LiFePO_4$ cells with IPG membranes activated with 1 M LiTFSI in EC:DEC (1:1 w/w) at (25 °C, 0.1 C rate, 2.5–4.0 V).

conductivity of ESM membranes increases with increasing PEO content, which is associated with the PEO crystalline-amorphous phase transition, which enhances the ion mobility and segmental motion of the polymer chains. Hence the Li ions coordinated with the 'O' atoms of PEO segments can be freed partially or fully which could lead to large number of charge carriers with improved charge migration. Higher ionic conductivity has been reported for a polymer blend containing higher PEO content [23].

It is seen that within the temperature range −20 to 70 °C, log σ vs 1/T curves for all the CPEs are slightly curved, therefore the activation energy for ionic conduction E_a can be obtained using the Vogel–Tamman–Fulcher (VTF) model $\{\sigma = \sigma_0\ T^{-1/2}\ \exp\ [(-E_a/R(T-T_0))]\}$ instead of the simple Arrhenius model ($\sigma = \sigma_0 \exp(-E_a/RT)$) used for the treatment of the linear plots. This indicates that conduction mechanism not only involves the increasing dissociation of lithium salt and lowering of ionic coupling but also the segmental motion of the polymer chains. There are two linear regions (Arrhenius behavior) between −20 and 10 and 10–70 °C with distinct change in slope typical of CPEs indicating different activation energies and conduction mechanism involved for the ion transport as function of temperature. The sharp decrease in conductivity below 10 °C is due to the freezing property of carbonate solvents in the electrolyte solution (EC:DEC) [5]. Compared to IPG membranes, the ionic conductivity of the ESM membrane increases more steeply beyond 30 °C, which is presumably due to the softening and melting of crystalline phase of PEO [5].

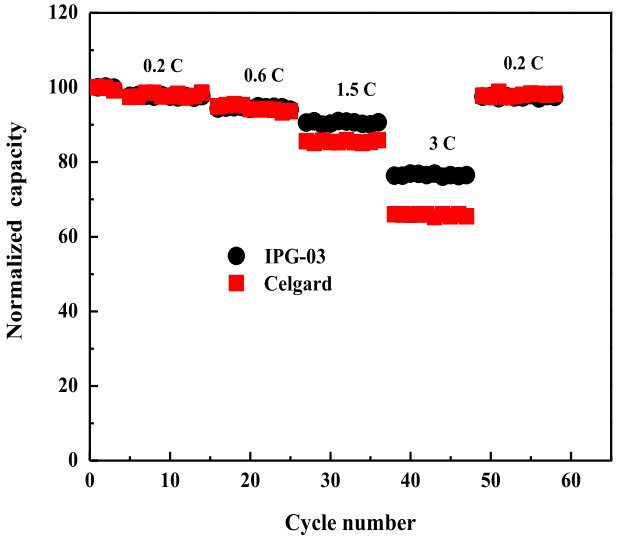

Fig. 10. Normalized rate capability of Li/CPE/$LiFePO_4$ cell with IPG-03 and Celgard (25 °C, 0.1–3 C rate, 2.5–4.0 V).

3.4. Electrochemical properties evaluation

3.4.1. Interfacial resistance and anodic stability

The formation of a stable solid electrolyte interface on the lithium metal that can conduct lithium ions freely and simultaneously avert any undesirable interaction between the electrolyte components and lithium is crucial for achieving good cycle performance. Fig. 6(a) and (b) illustrates the complex impedance response of Li/CPE/Li symmetric cells and their impedance initially and after 12 days storage measured at open circuit potential at ambient temperature. Impedance spectrum shows a distorted semi-circle in the middle frequency range, and its expansion with storage time indicates the formation and growth of passivation layer at the interface of CPE and lithium metal electrode. The growth of passivation layer is associated with the decomposition of the electrolyte or the reaction between the electrolyte and the Li-metal electrode [1,35,36]. The real axis intercept at the high frequency end represents the bulk electrolyte resistance (R_b) while the intercept at the low frequency end represents the charge transfer kinetics and the growth of the SEI layer. The intercept at the lower frequency end (R_f) is the resistance of the interface between lithium and the electrolyte. The initial R_b values (Fig 6a) follow the order IPG-03 < IPG-02 < IPG-01 and the values are well in agreement with the low R_b observed for these electrolytes in SS/CPE/SS symmetric cells. The R_b values are low and are in the range of 1.4–5 Ω for the CPEs having an area of ~2 cm^2, thus, denoting a high ionic conductivity, as discussed earlier in Sec. 3.3.

Fig. 6(a) shows the initial interfacial (R_i) resistance of the electrolytes which follows the order IPG-01 > IPG-02 > IPG-03 with values in the close range of 11–23 Ω, while ESM-03 shows an R_i of 22 Ω. No significant difference in initial interfacial resistance is observed for the electrolyte based on the composite membrane before and after leaching out the PEO. Fig. 6(b) shows the interfacial resistance after 12 days of storage at room temperature. It is seen that there is no significant change in the R_b values with storage time, which shows that there is no leakage or loss of electrolyte from the pores indicating that high ionic conductivity and dimensional stability of the electrolyte is maintained. It is observed that after 12 days of storage the cell with ESM-03 showed R_f value of ~85 Ω which is about 20–60% higher than CPEs based on IPG membranes. After a period of 12 days storage the R_f value (Ω) follows the order IPG-03 (53) < IPG-02 (59), IPG-01 (71)<ESM-03 (85) which is 208–381% higher than R_i.

Fig. 7 shows the change in interfacial resistance as a function of storage time. The R_f for all the CPEs increase with storage time, denoting the growth and stabilization of the SEI layer. Progressive expansion of the middle frequency range semi circle in the impedance spectrum reveals the formation and growth of passivation layer at the CPE and lithium metal electrode interface with time. The increase in interfacial resistance with storage time may also be associated with degradation of physical contact between the electrode and CPE [22]. After the initial enhancement in impedance, due to the growth of the passivation layer, the layer characteristics get stabilized within 8 days. Compared to ESM membranes, the better interfacial properties of the IPG membranes with storage time is due to larger surface area due to the higher porosity, thinning of fiber diameter, increased surface roughness

due to the preferential leaching out of PEO leading to better adhesion, good compatibility with the electrolyte and higher ionic conductivity.

The electrochemical stability window of the electrolyte is an important parameter to determine the practical application of the electrolyte in a lithium ion battery. The voltage corresponding to the onset of a steady and continuous increase of current indicates the electrochemical stability limit of the electrolyte [37]. Fig. 8 shows the LSV curves of the IPG membranes. It is seen that all the membranes have anodic stability > 5 V, rendering them suitable for use with most of the common cathode materials used in lithium ion batteries. The high anodic stability may be due to the excellent affinity of the membrane to the carbonate based liquid electrolyte which partially swells the fibers. The surface roughness of the fibers also leads to better contact of the electrolyte to lithium surface which leads to better anodic stability. It is reported that LAGP particles can act as a surface stabilizer and enhance the electrochemical oxidation stability of the composite polymer electrolytes [28,37].

3.4.2. Evaluation in Li/LiFePO$_4$ cell

To test the practical applicability of the IPG polymer electrolyte, it is tested in Li/CPE/LiFePO$_4$ cell. LiFePO$_4$ has high theoretical capacity (170 mAh g^{-1}), flat operating voltage of 3.4 V and excellent cycling properties at low *C*-rate. Additionally, with its ease of preparation, non-toxicity and low cost, it is a preferred cathode material for lithium ion batteries. Li/CPE/LiFePO$_4$ cells are assembled and cycled at 0.1–3 C rate between 2.5 and 4 V at room temperature. Fig. 9 shows the discharge capacity vs. cycle number for the cells based on IPG membranes cycled at 0.1 C. The discharge capacity of the cells comprised of composite polymer electrolyte follows the order IPG-03 > IPG-02 > IPG-01. The difference in capacity may be due to the difference in ionic conductivity of the CPEs as discussed in the previous section (Sec. 3.3). It is observed that all the cells show relatively stable performance without significant capacity fading for 50 cycles. After 50 cycles the cells delivered a discharge capacity of 126, 137 and 150 mAh g^{-1} respectively for the cells based on IPG-03, IPG-02 and IPG-01 respectively. The observed capacity fade may be due to the progressive decomposition and/or leakage of the electrolyte. Also the structural characteristics and composition of cathode materials play a vital role on the capacity of the cell and cycling performance [38,39]. The capacity retention ratios of the cells are found to be 98 ± 1%. The relatively stable performance with good capacity retention proves the suitability of the IPG polymer electrolytes for application in LIBs.

The electrochemical performance of Li/LiFePO$_4$ cells with the IPG electrolytes at different current densities is compared with conventional Celgard separator and shown in Fig. 10. The cells are cycled between 0.1 and 3 C-rate for 10 cycles each continuously and then at 0.2 C rate for 10 cycles. All the cells showed good discharge capacity and cycling performance even at higher *C*-rate and retain similar capacity after the current density is changed back to 0.2 C-rate after 40 cycles, which clearly demonstrates high capacity retention of the cells. The capacity is normalized by the capacity obtained at 0.1 C rate to study the effect of porous morphology on the performance. The nature of the porous membrane has been reported to have a poor effect on the cycling test performances at low rates [40,41]. At low *C* rates (0.1–0.6 C), it is seen that Celgard and IPG membranes have similar capacities. But at higher *C* rates (1.5–3.0 C), the IPG membrane shows considerably higher capacity compared to Celgard. The lower interfacial resistance, higher porosity, electrolyte uptake, pore structure and ionic conductivity of the IPG electrolyte is responsible for the higher normalized capacity. At a fixed thickness, a less conductive electrolyte (Celgard) results in an increase of the ohmic drop and the ion concentration gradient in the electrolyte leading to lower capacity [40,41]. The lowering of capacity at high C rate is also attributed to the nature of the electrode. The LiFePO$_4$ cathode material is known to suffer the limitation of lower performance at higher C-rate and reduced temperatures due to slow Li^+ ion diffusion at the solid, two-phase boundary of LiFePO$_4$/FePO$_4$ [39].

4. Conclusions

Non-woven fibrous mats of PEO/PVdF-LAGP composite are prepared. The electrospinning parameters are controlled to get membranes having uniform fibers with bead-free morphology, high porosity and uniform fiber distribution. The membranes are subjected to pre-treatment to generate porosity in-situ. The suitability of the membrane as host matrix for the preparation of polymer electrolytes and its application in lithium ion batteries are explored. Porosity, electrolyte uptake measurement, thermal and mechanical studies and complex AC-impedance studies are conducted to examine the properties of the composite polymer electrolyte membranes. The prepared composite polymer electrolytes exhibit high electrolyte uptake, porosity and ionic conductivity. The in-situ porosity generation significantly improves the electrochemical performance when compared to pristine membranes. It is seen that incorporation of glass ceramic helps to improve thermal and mechanical properties, thus ensuring good handleability. The electrolytes perform well with stable charge–discharge characteristics when evaluated as separator-cum-electrolyte in a lithium-ion cell. IPG membranes outperform ESM membranes indicating in-situ porosity generation has a more pronounced effect compared to blending of PEO. Thus the present methodology can be extended to prepare a variety of polymer electrolytes to achieve required characteristics by choosing the appropriate combination of materials.

Acknowledgment

This work was supported by funding from the National Research Foundation (501100001321), Competetive research Program, grant number NRF2011 NRF-CRP001-105. The authors are thankful to Dr. Nutan Gupta and Dr. Chui Ling, School of Materials Science and Engineering, Nanyang Technological University, Singapore, for their kind help to synthesis the glass ceramic used in this study.

References

[1] S. Ahmad, Ionics 15 (2009) 309–321.
[2] A. Manuelstephan, Eur. Polym. J. 42 (2005) 21–42.
[3] Z.H. Li, Q.Z. Xiao, P. Zhang, H.P. Zhang, Y.P. Wu, T. Van Ree, Funct. Mater. Lett. 01 (2008) 139–143.
[4] P.V. Wright, MRS Bull. (2002) 597–602.
[5] R. Prasanth, N. Shubha, H.H. Hng, M. Srinivasan, J. Power Sources 245 (2014) 283–291.
[6] Y. Saito, A. Manuel Stephan, H. Kataoka, Solid State Ionics 160 (2003) 149–153.
[7] N.T. Kalyana Sundaram, A. Subramania, Electrochim. Acta 52 (2007) 4987–4993.
[8] A. Zalewska, M. Walkowiak, L. Niedzicki, T. Jesionowski, N. Langwald, Electrochim. Acta 55 (2010) 1308–1313.
[9] N. Wu, Q. Cao, X. Wang, S. Li, X. Li, H. Deng, J. Power Sources 196 (2011) 9751–9756.
[10] W. Wieczorek, A. Zalewska, D. Raducha, Z. Florjanczyk, J. Stevens, J. Phys. Chem. B 102 (1998) 352–360.
[11] P. Raghavan, X. Zhao, J. Manuel, G.S. Chauhan, J.H. Ahn, H.S. Ryu, H.J. Ahn, K.W. Kim, C. Nah, Electrochim. Acta 55 (2010) 1347–1354.
[12] P. Raghavan, J.W. Choi, J.H. Ahn, G. Cheruvally, G.S. Chauhan, H.J. Ahn, C. Nah, J. Power Sources 184 (2008) 437–443.
[13] P. Raghavan, X. Zhao, J. Kim, J. Manuel, G. Chauhan, J. Ahn, C. Nah, Electrochim. Acta 54 (2008) 228–234.

[14] A. Manuel Stephan, K.S. Nahm, T. Prem Kumar, M.A. Kulandainathan, G. Ravi, J. Wilson, J. Power Sources 159 (2006) 1316–1321.
[15] B. Scrosati, C.A. Vincent, MRS Bull. (2000) 28–30.
[16] A. Du Pasquier, P.C. Warren, D. Culver, A.S. Gozdz, G.G. Amatucci, J.M. Tarascon, Solid State Ionics 135 (2000) 249–257.
[17] C.J. Leo, A.K. Thakur, G.V. Subba Rao, B.V.R. Chowdari, J. Power Sources 115 (2003) 295–304.
[18] M. Kotobuki, K. Hoshina, Phosphorus Res. Bull. 24 (2011) 61–63.
[19] M. Zhang, K. Takahashi, N. Imanishi, Y. Takeda, O. Yamamoto, B. Chi, J. Pu, J. Li, J. Electrochem. Soc. 159 (2012) A1114–A1119.
[20] S.W. Choi, S.M. Jo, W.S. Lee, Y.R. Kim, Adv. Mater. 15 (2003) 2027–2031.
[21] J.R. Kim, S.W. Choi, S.M. Jo, W.S. Lee, B.C. Kim, J. Electrochem. Soc. 152 (2005) A295–A300.
[22] N. Shubha, R. Prasanth, H.H. Hoon, M. Srinivasan, Mater. Res. Bull. 48 (2013) 526–537.
[23] M. Jacob, S. Prabaharan, S. Radhakrishna, Solid State Ionics 104 (1997) 267–276.
[24] J. Choi, G. Cheruvally, Y. Kim, J. Kim, J. Manuel, P. Raghavan, J. Ahn, K. Kim, H. Ahn, D. Choi, Solid State Ionics 178 (2007) 1235–1241.
[25] M. Morita, H. Noborio, N. Yoshimoto, M. Ishikawa, Solid State Ionics 177 (2006) 715–720.
[26] H. Sun, Y. Takeda, N. Imanishi, J. Electrochem. Soc. 147 (2000) 2462–2467.
[27] S.H. Chung, Y. Wang, L. Persi, F. Croce, S.G. Greenbaum, B. Scrosati, E. Plichta, J. Power Sources 97–98 (2001) 644–648.
[28] Y. Liang, Z. Lin, Y. Qiu, X. Zhang, Electrochim. Acta 56 (2011) 6474–6480.
[29] Z. Li, G. Su, X. Wang, D. Gao, Solid State Ionics 176 (2005) 1903–1908.
[30] M.A.K.L. Dissanayake, P.A.R.D. Jayathilaka, R.S.P. Bokalawala, I. Albinsson, B.E. Mellander, J. Power Sources 119–121 (2003) 409–414.
[31] C.R. Mariappan, C. Yada, F. Rosciano, B. Roling, J. Power Sources 196 (2011) 6456–6464.
[32] D. Safanama, D. Damiano, R.P. Rao, S. Adams, Solid State Ionics 5 (2013) 1–5.
[33] H. Cheng, C. Zhu, B. Huang, M. Lu, Y. Yang, Electrochim. Acta 52 (2007) 5789–5794.
[34] G. Cheruvally, J.K. Kim, J.W. Choi, J.H. Ahn, Y.J. Shin, J. Manuel, P. Raghavan, K.W. Kim, H.J. Ahn, D.S. Choi, C.E. Song, J. Power Sources 172 (2007) 863–869.
[35] F. Dias, L. Plomp, J. Veldhuis, J. Power Sources 88 (2000) 169–191.
[36] K. Xu, Chem. Rev. 104 (2004) 4303–4417.
[37] Y. Liang, L. Ji, B. Guo, Z. Lin, Y. Yao, Y. Li, M. Alcoutlabi, Y. Qiu, X. Zhang, J. Power Sources 196 (2011) 436–441.
[38] Z. Li, D. Zhang, F. Yang, J. Mater. Sci. 44 (2009) 2435–2443.
[39] A.K. Padhi, K.S. Nanjundaswamy, J.B. Goodenough, J. Electrochem. Soc. 144 (1997) 1188–1194.
[40] D. Djian, F. Alloin, S. Martinet, H. Lignier, J. Power Sources 187 (2009) 575–580.
[41] D. Djian, F. Alloin, S. Martinet, H. Lignier, J.Y. Sanchez, J. Power Sources 172 (2007) 416–421.